

Study of $e^+e^- \rightarrow \pi^+\pi^-\Upsilon(1D)$ at Belle II

The Belle II Collaboration



M. Abumusabh , I. Adachi , A. Aggarwal , L. Aggarwal , H. Ahmed , Y. Ahn ,
 H. Aihara , S. Alghamdi , M. Alhakami , A. Aloisio , N. Althubiti , K. Amos ,
 M. Angelsmark , N. Anh Ky , C. Antonioli , D. M. Asner , H. Atmacan ,
 T. Aushev , R. Ayad , V. Babu , H. Bae , N. K. Baghel , S. Bahinipati ,
 P. Bambade , Sw. Banerjee , M. Barrett , M. Bartl , J. Baudot , A. Baur ,
 A. Beaubien , F. Becherer , J. Becker , J. V. Bennett , F. U. Bernlochner ,
 V. Bertacchi , M. Bertemes , E. Bertholet , M. Bessner , S. Bettarini ,
 F. Bianchi , T. Bilka , D. Biswas , A. Bobrov , D. Bodrov , A. Bondar ,
 G. Bonvicini , J. Borah , A. Boschetti , A. Bozek , M. Bračko , P. Branchini ,
 R. A. Briere , T. E. Browder , A. Budano , S. Bussino , Q. Campagna ,
 M. Campajola , G. Casarosa , C. Cecchi , M.-C. Chang , P. Cheema , L. Chen ,
 B. G. Cheon , C. Cheshta , H. Chetri , K. Chilikin , K. Chirapatpimol ,
 H.-E. Cho , K. Cho , S.-J. Cho , S.-K. Choi , S. Choudhury , S. Chutia ,
 J. Cochran , J. A. Colorado-Caicedo , I. Consigny , L. Corona , J. X. Cui ,
 E. De La Cruz-Burelo , S. A. De La Motte , G. De Nardo , G. De Pietro ,
 R. de Sangro , M. Destefanis , S. Dey , R. Dhayal , A. Di Canto ,
 J. Dingfelder , Z. Doležal , I. Domínguez Jiménez , T. V. Dong , X. Dong ,
 M. Dorigo , K. Dugic , G. Dujany , P. Ecker , D. Epifanov , J. Eppelt ,
 R. Farkas , P. Feichtinger , T. Ferber , T. Fillinger , C. Finck , G. Finocchiaro ,
 F. Forti , A. Frey , B. G. Fulsom , A. Gabrielli , A. Gale , E. Ganiev , R. Garg ,
 G. Gaudino , V. Gaur , V. Gautam , A. Gaz , A. Gellrich , G. Ghevondyan ,
 D. Ghosh , H. Ghumaryan , R. Giordano , A. Giri , P. Gironella Gironell ,
 B. Gobbo , R. Godang , W. Gradl , E. Graziani , D. Greenwald , Y. Guan ,
 K. Gudkova , I. Haide , Y. Han , H. Hayashii , S. Hazra , C. Hearty ,
 A. Heidelberg , G. Heine , I. Heredia de la Cruz , M. Hernández Villanueva ,
 T. Higuchi , M. Hoek , M. Hohmann , R. Hoppe , P. Horak , C.-L. Hsu ,
 T. Humair , T. Iijima , K. Inami , N. Ipsita , A. Ishikawa , R. Itoh ,
 M. Iwasaki , P. Jackson , D. Jacobi , W. W. Jacobs , E.-J. Jang , Q. P. Ji ,
 S. Jia , Y. Jin , A. Johnson , J. Kandra , K. H. Kang , G. Karyan , F. Keil ,
 C. Ketter , C. Kiesling , D. Y. Kim , H. Kim , J.-Y. Kim , K.-H. Kim ,
 K. Kinoshita , P. Kodyš , T. Koga , S. Kohani , A. Korobov , S. Korpar ,
 E. Kovalenko , R. Kowalewski , P. Križan , P. Krokovny , T. Kuhr , Y. Kulii

D. Kumar , R. Kumar , K. Kumara , S. Kurokawa , A. Kuzmin , Y.-J. Kwon , S. Lacaprara , T. Lam , J. S. Lange , T. S. Lau , M. Laurenza , R. Leboucher , F. R. Le Diberder , H. Lee , M. J. Lee , C. Lemettais , P. Leo , H.-J. Li , L. K. Li , Q. M. Li , S. X. Li , W. Z. Li , Y. Li , Y. B. Li , Y. P. Liao , J. Libby , J. Lin , Z. Liptak , M. H. Liu , Q. Y. Liu , Y. Liu , Z. Q. Liu , D. Liventsev , S. Longo , A. Lozar , T. Lueck , C. Lyu , J. L. Ma , Y. Ma , M. Maggiora , S. P. Maharana , R. Maiti , G. Mancinelli , R. Manfredi , E. Manoni , M. Mantovano , D. Marcantonio , S. Marcello , M. Marfoli , C. Marinas , C. Martellini , A. Martens , T. Martinov , L. Massaccesi , M. Masuda , D. Matvienko , S. K. Maurya , M. Maushart , F. Mawas , J. A. McKenna , Z. Mediankin Gruberová , R. Mehta , F. Meier , D. Meleshko , M. Merola , C. Miller , M. Mirra , K. Miyabayashi , H. Miyake , R. Mizuk , G. B. Mohanty , S. Moneta , H.-G. Moser , Th. Muller , R. Mussa , I. Nakamura , M. Nakao , H. Nakazawa , Y. Nakazawa , M. Naruki , Z. Natkaniec , A. Natochii , M. Nayak , M. Neu , M. Niiyama , S. Nishida , R. Nomaru , A. Novosel , S. Ogawa , R. Okubo , H. Ono , F. Otani , P. Pakhlov , G. Pakhlova , A. Panta , S. Pardi , K. Parham , J. Park , K. Park , S.-H. Park , A. Passeri , S. Patra , S. Paul , T. K. Pedlar , R. Pestotnik , M. Piccolo , L. E. Piilonen , P. L. M. Podesta-Lerma , T. Podobnik , A. Prakash , C. Praz , S. Prell , E. Prencipe , M. T. Prim , S. Privalov , I. Prudiiev , M. V. Purohit , H. Purwar , S. Raiz , K. Ravindran , J. U. Rehman , M. Reif , S. Reiter , L. Reuter , D. Ricalde Herrmann , I. Ripp-Baudot , G. Rizzo , S. H. Robertson , J. M. Roney , A. Rostomyan , N. Rout , S. Saha , L. Salutari , D. A. Sanders , S. Sandilya , L. Santelj , C. Santos , V. Savinov , B. Scavino , S. Schneider , K. Schoenning , C. Schwanda , Y. Seino , K. Senyo , J. Serrano , M. E. Sevier , C. Sfienti , W. Shan , C. P. Shen , X. D. Shi , T. Shillington , T. Shimasaki , J.-G. Shiu , D. Shtol , A. Sibidanov , F. Simon , J. Skorupa , R. J. Sobie , M. Sobotzik , A. Soffer , A. Sokolov , E. Solovieva , S. Spataro , K. Špenko , B. Spruck , M. Starič , P. Stavroulakis , S. Stefkova , R. Stroili , J. Strube , M. Sumihama , N. Suwonjandee , M. Takizawa , K. Tanida , F. Tenchini , F. Testa , A. Thaller , T. Tien Manh , O. Tittel , R. Tiwary , E. Torassa , K. Trabelsi , F. F. Trantou , I. Tsaklidis , I. Ueda , K. Unger , Y. Unno , K. Uno , S. Uno , Y. Ushiroda , S. E. Vahsen , R. van Tonder , K. E. Varvell , M. Veronesi , V. S. Vismaya , L. Vitale , V. Vobbilisetti , R. Volpe , M. Wakai , S. Wallner , M.-Z. Wang , A. Warburton , M. Watanabe , S. Watanuki , C. Wessel , E. Won , Y. Xie , X. P. Xu , B. D. Yabsley , W. Yan , W. Yan , J. Yelton , K. Yi , J. H. Yin , K. Yoshihara , J. Yuan , Y. Yusa , L. Zani , F. Zeng , M. Zeyrek , B. Zhang , V. Zhilich , J. S. Zhou , Q. D. Zhou , L. Zhu , R. Žlebčik

ABSTRACT: The bottomonium spectrum, consisting of bound states of a b quark and an anti- b quark, provides an excellent laboratory for probing quantum chromodynamics in the non-perturbative regime. While S and P-wave bottomonium states are well studied experimentally, information on D-wave states remains scarce. We search for D-wave bottomonium state via the decay of a vector bottomonium-like state $\Upsilon(10753)$ in the reaction $e^+e^- \rightarrow \pi^+\pi^-\Upsilon(1D)$, using 19.6 fb^{-1} of data collected with the Belle II detector at center-of-mass energies $\sqrt{s} = 10.653, 10.701, 10.745, \text{ and } 10.805 \text{ GeV}$, in the vicinity of the $\Upsilon(10753)$ resonance. No significant signals are observed. Upper limits at the 90% credibility level are set on the products of the cross sections and branching fractions, $\sigma[e^+e^- \rightarrow \pi^+\pi^-\Upsilon_2(1D)] \times \mathcal{B}(\Upsilon_2(1D) \rightarrow \gamma\chi_{b1})$ and $\sigma[e^+e^- \rightarrow \pi^+\pi^-\Upsilon_3(1D)] \times \mathcal{B}(\Upsilon_3(1D) \rightarrow \gamma\chi_{b2})$, at each center-of-mass energy.

Contents

1	Introduction	1
2	Belle II Detector and Data Samples	3
3	Event Selection and Background Study	4
4	Signal Extraction	6
5	Cross Section Measurement	7
6	Systematic Uncertainty	10
7	Discussion	13
8	Summary	13

1 Introduction

Bottomonium states, composed of a bottom quark (b) and an antiquark (\bar{b}), offer a vital platform for probing quantum chromodynamics (QCD) in the non-perturbative regime [1]. The substantial mass of the bottom quark ($\sim 4.18 \text{ GeV}/c^2$) leads to non-relativistic dynamics, positioning bottomonium as an ideal system for validating potential models, such as the Godfrey-Isgur relativized quark model [2] and the Cornell potential model [3]. The bottomonium spectrum includes S-wave states (with orbital angular momentum $L = 0$), P-wave states ($L = 1$), D-wave states ($L = 2$) and higher orbital excitations. While S-wave and P-wave states have been extensively studied [4], much less is known about D-wave states. Completing the bottomonium spectrum not only tests lattice QCD calculations but also rigorously evaluates our comprehension of bottomonium within the quark model framework [1, 2, 5, 6], potentially revealing unexpected states that could hint at exotic structures.

The $1D$ states of the D-wave bottomonia, characterized by radial quantum number $n = 1$, include the spin-triplet configurations (1^3D_J) with total angular momentum $J = 1, 2, 3$ and the spin-singlet state (1^1D_2) with $J = 2$. The CLEO Collaboration reported the first observation for the $\Upsilon_J(1D)$ states (corresponding to the 1^3D_J) via the radiative decay $\Upsilon(3S) \rightarrow \gamma\gamma\Upsilon_J(1D)$ [7], favoring a $J = 2$ assignment among $J = 1, 2, 3$. This observation was subsequently confirmed by the BaBar Collaboration through the same decay process [8], providing the first definitive identification of the $\Upsilon_2(1D)$ state. Both experiments yielded inconclusive evidence for the $\Upsilon_1(1D)$ (1^3D_1) and $\Upsilon_3(1D)$ (1^3D_3) states. A theoretical prediction from the nonrelativistic screened-potential model estimates only

small mass differences of $M_{\Upsilon_3(1D)} - M_{\Upsilon_2(1D)} \approx 4 \text{ MeV}$ and $M_{\Upsilon_2(1D)} - M_{\Upsilon_1(1D)} \approx 7 \text{ MeV}$ [9], implying that the observed signals may represent a composite of contributions from the $\Upsilon_1(1D)$, $\Upsilon_2(1D)$, and $\Upsilon_3(1D)$ states. Additional experimental insights into the D-wave states have emerged from the Belle experiment, which saw a low-significance (2.4σ) excess of the decay $\Upsilon(5S) \rightarrow \pi^+\pi^-\Upsilon_J(1D)$ ($J = 1, 2, 3$) in an inclusive analysis of $\Upsilon(5S) \rightarrow \pi^+\pi^-X$ decays [10]. However, these analyses did not resolve the individual contributions of the $\Upsilon_1(1D)$, $\Upsilon_2(1D)$, and $\Upsilon_3(1D)$ states, highlighting the necessity for further experimental efforts to elucidate their distinct properties.

In addition, exploring the $\Upsilon_J(1D)$ states in decays from other resonances beyond $\Upsilon(3S)$ and $\Upsilon(5S)$ presents an intriguing avenue for discovery, potentially revealing new production mechanisms and transition dynamics in the bottomonium spectrum. The $\Upsilon(10753)$, a vector bottomonium-like state with quantum numbers ($J^{PC} = 1^{--}$), was first observed in e^+e^- collisions through the processes $e^+e^- \rightarrow \pi^+\pi^-\Upsilon(nS)$ ($n = 1, 2, 3$) by the Belle Collaboration [11], with further confirmation and refined measurements by Belle II [12–15]. Additionally, its decay to $\omega\chi_{b1,b2}$, where χ_{b1} and χ_{b2} are P-wave bottomonium states, has been observed at Belle II [14], suggesting that the $e^+e^- \rightarrow \omega\chi_{b1,b2}$ process observed near $\Upsilon(5S)$ from Belle [16] could be due to the tail of the $\Upsilon(10753)$. The production rate of $\omega\chi_{bJ}$ compared to $\pi^+\pi^-\Upsilon(nS)$ at the $\Upsilon(10753)$ significantly exceeds that at the $\Upsilon(5S)$, despite their identical quantum numbers ($J^{PC} = 1^{--}$) and small mass difference ($\sim 110 \text{ MeV}/c^2$), which may indicate distinctly different internal structures for $\Upsilon(10753)$ and $\Upsilon(5S)$ [14]. However, experimental data on the $\Upsilon(10753)$ remain limited, leaving its nature unresolved.

There is a broad range of theoretical interpretations for the $\Upsilon(10753)$, reflecting the complexity of its classification. Conventional bottomonium models propose it to be a higher radial excitation [17–26]. However, its measured mass [11, 12, 14] does not correspond to predicted masses of standard radial excitations [2] (e.g., $\Upsilon(5S)$ or $\Upsilon(6S)$). Furthermore, its decay rate to $\omega\chi_{b1,b2}$ [14] is significantly enhanced compared to that of the $\Upsilon(5S)$ [16]. Alternative hypotheses suggest it could be a hybrid state [27, 28], incorporating gluonic excitations, or a tetraquark [29–32]. These models predict distinct decay patterns and branching fractions, particularly for hadronic transitions, which could reveal signatures of exotic configurations.

The decay $\Upsilon(10753) \rightarrow \pi^+\pi^-\Upsilon_J(1D)$ is kinematically feasible due to the mass difference of approximately 588 MeV, sufficient to produce two charged pions. In conventional bottomonium, dipion transitions are well-established, as seen in $\Upsilon(nS) \rightarrow \pi^+\pi^-\Upsilon(mS)$ ($n > m; n = 2, 3, 4; m = 1, 2$) decays [4]. If $\Upsilon(10753)$ is a conventional state, its decay rate to $\Upsilon_J(1D)$ should be consistent with predictions from potential models or non-relativistic QCD [1, 2, 5, 6]. Conversely, exotic interpretations may yield suppressed or enhanced rates, or distinct dipion mass spectra, due to different wave functions or selection rules [29]. The study of $\Upsilon(10753) \rightarrow \pi^+\pi^-\Upsilon_J(1D)$ decay is critical for testing these models and elucidating the $\Upsilon(10753)$'s nature.

In this analysis, we search for the processes $e^+e^- \rightarrow \Upsilon(10753) \rightarrow \pi^+\pi^-\Upsilon_J(1D)$ ($J = 2, 3$) at Belle II. The $\Upsilon_J(1D)$ candidates are reconstructed via the decays $\Upsilon_J(1D) \rightarrow \gamma\chi_{bJ'}$ ($J' = 0, 1, 2$), with $\chi_{bJ'} \rightarrow \gamma\Upsilon(1S)$ and $\Upsilon(1S) \rightarrow \ell^+\ell^-$ ($\ell = e, \mu$). By exploring these

decay channels, we aim to probe the properties of the $\Upsilon_J(1D)$ states and provide new insights into the internal structure of the $\Upsilon(10753)$ resonance, advancing our understanding of bottomonium spectroscopy and the potential existence of exotic hadrons beyond bottomonium. The $J = 1$ case, corresponding to the $\Upsilon_1(1D)$ state, is excluded from this study. Theoretical predictions indicate that its decay favors $\gamma\chi_{b0}$ [9], but the branching fraction for $\chi_{b0} \rightarrow \gamma\Upsilon(1S)$ is exceedingly small [4] which results in limited sensitivity for this channel. For $\Upsilon_2(1D)$ ($J = 2$), theoretical predictions suggest that it primarily decays to $\gamma\chi_{b1}$ or $\gamma\chi_{b2}$, with the branching fraction for $\Upsilon_2(1D) \rightarrow \gamma\chi_{b1} \rightarrow \gamma\gamma\Upsilon(1S)$ being approximately six times greater than that for $\Upsilon_2(1D) \rightarrow \gamma\chi_{b2} \rightarrow \gamma\gamma\Upsilon(1S)$ [9]. To maximize sensitivity by focusing on the mode with the highest expected signal yield relative to background, we exclusively consider the χ_{b1} decay for the $\Upsilon_2(1D)$ search. In the case of $\Upsilon_3(1D)$ ($J = 3$), the branching fraction for $\Upsilon_3(1D) \rightarrow \gamma\chi_{b2}$ approaches 100% [9], leading to a focus solely on this χ_{b2} decay channel. We measure the products of the cross sections and branching fractions for $\sigma[e^+e^- \rightarrow \pi^+\pi^-\Upsilon_2(1D)] \times \mathcal{B}(\Upsilon_2(1D) \rightarrow \gamma\chi_{b1})$ and $\sigma[e^+e^- \rightarrow \pi^+\pi^-\Upsilon_3(1D)] \times \mathcal{B}(\Upsilon_3(1D) \rightarrow \gamma\chi_{b2})$.

2 Belle II Detector and Data Samples

The Belle II experiment is located at SuperKEKB, which collides electrons and positrons at and near the $\Upsilon(4S)$ resonance [33]. The Belle II detector [34] has a cylindrical geometry and includes a two-layer silicon-pixel detector (PXD) surrounded by a four-layer double-sided silicon-strip detector (SVD) [35] and a 56-layer central drift chamber (CDC). Position information from these detectors is used to reconstruct the trajectories of charged particles [36]. Only one sixth of the second layer of the PXD was installed for the data analyzed here. The symmetry axis of these detectors, defined as the z -axis, is almost coincident with the direction of the electron beam. Surrounding the CDC, which also provides dE/dx energy-loss measurements, is a time-of-propagation counter (TOP) [37] in the central region and an aerogel-based ring-imaging Cherenkov counter (ARICH) in the forward region. These detectors provide charged-particle identification. The TOP and ARICH are surrounded by an electromagnetic calorimeter (ECL) consisting of CsI(Tl) crystals that covers the central, forward and backward regions, primarily providing energy and timing measurements for photons and electrons. Outside of the ECL is a superconducting solenoid magnet. The magnet provides a 1.5 T magnetic field that is parallel to the z -axis. Its flux return is instrumented with resistive-plate chambers and plastic scintillator modules to detect muons, K_L^0 mesons, and neutrons.

This analysis is performed using the Belle II Analysis Software Framework [38, 39]. The data sample corresponds to an integrated luminosity of 19.6 fb^{-1} , recorded in November 2021 at center-of-mass energies near 10.75 GeV ($\sqrt{s} = 10.653, 10.701, 10.745, \text{ and } 10.805 \text{ GeV}$). These energies were chosen to probe the $\Upsilon(10753)$ resonance.

The Monte Carlo (MC) simulation samples are generated using a GEANT4-based software package [40], which incorporates a detailed geometric description of the Belle II detector and its response. These simulations are essential for evaluating detection efficiencies, optimizing event selection criteria, and estimating background contributions.

At each center-of-mass energy, MC events for the signal processes $e^+e^- \rightarrow \pi^+\pi^-\Upsilon_J(1D)$ ($J = 2, 3$), followed by $\Upsilon_J(1D) \rightarrow \gamma\chi_{b1}$ or $\gamma\chi_{b2}$, are produced using the EVTGEN package [41]. The dynamics of the $\pi^+\pi^-\Upsilon_J(1D)$ production and the $\Upsilon_J(1D)$ decay are modeled using a phase-space (PHSP) approach. Initial-state radiation (ISR) is simulated at next-to-leading order accuracy in quantum electrodynamics using PHOKHARA [42], with the initial input cross section line-shape proportional to $\frac{1}{s}$. The maximum energy of ISR photons is set by the production threshold of the $\pi^+\pi^-\Upsilon_J(1D)$ system. Final-state radiation from charged particles is incorporated using PHOTOS [43].

To investigate specific background sources that yield similar or identical final state particles, MC samples are generated for processes including $e^+e^- \rightarrow \omega[\rightarrow \pi^+\pi^-\pi^0]\chi_{b1,b2}[\rightarrow \gamma\Upsilon(1S)]$, $e^+e^- \rightarrow \gamma_{\text{ISR}}\Upsilon(2S)[\rightarrow \pi^+\pi^-\Upsilon(1S)]$, and $e^+e^- \rightarrow \eta[\rightarrow \gamma\gamma]\Upsilon(2S)[\rightarrow \pi^+\pi^-\Upsilon(1S)]$. Additional simulated samples of continuum $e^+e^- \rightarrow q\bar{q}$ ($q = u, d, s, c$) processes, low-multiplicity quantum electrodynamic processes (e.g., Bhabha scattering, $\mu^+\mu^-(\gamma)$, $\tau^+\tau^-(\gamma)$, and $\gamma\gamma$) [44, 45], ISR-produced hadron pair processes [46], and four-track processes with at least one lepton pair [47, 48] are examined to assess possible background contributions. Backgrounds from $B\bar{B}$ production are negligible at the center-of-mass energies studied.

3 Event Selection and Background Study

Events are selected online using a hardware trigger that leverages information from the CDC and the ECL [49]. In the offline analysis, photon candidates are identified from clusters in the ECL within the angular acceptance of the CDC, spanning the polar angle range $17^\circ < \theta < 150^\circ$. Each cluster must satisfy a quality condition where the sum of weights w_i ($w_i \leq 1$, where w_i refers to the energy-weighted contribution from the i -th crystal associated with this cluster) of all contributing crystals exceeds 1.5. This sum is equal to the number of crystals in non-overlapping clusters but can be non-integer for energy-shared clusters. The deposited energy in the cluster must exceed region-specific thresholds: 20 MeV in the barrel region, 22.5 MeV in the forward endcap region, or 20 MeV in the backward endcap region of the ECL. In the signal process, typical photon energies in the laboratory frame range from 100 to 600 MeV, resulting in no efficiency loss due to these thresholds, as confirmed by MC simulations.

Charged particles are identified using offline selection criteria applied to variables such as impact parameter, momentum, and ECL cluster energy. To ensure a track originates from the e^+e^- interaction point, we impose constraints: $\sqrt{d_x^2 + d_y^2} < 2.0$ cm and $|d_z| < 4.0$ cm, where d_x , d_y , and d_z are the coordinates in the x , y , and z directions, respectively, for the point (on the track) with the closest approach to the interaction point (determined using di-muon events). Pion (π^\pm) and lepton (ℓ^\pm) candidates are distinguished by their momenta: $p(\pi^\pm) < 1.0$ GeV and $p(\ell^\pm) > 1.0$ GeV, reflecting the kinematic properties of the signal process. Lepton identification exploits the fact that electrons typically deposit most of their energy in the ECL, whereas muons deposit little. The e^\pm (μ^\pm) candidates are therefore differentiated based on ECL cluster energy: $E_{\text{cluster}}(e^\pm) > 1.0$ GeV and $E_{\text{cluster}}(\mu^\pm) < 1.0$ GeV. In the signal processes, MC simulations indicate that the event-level efficiencies are 100.0% for identifying $\pi^+\pi^-$, 97.4% for the e^+e^- , and 96.7% for the

$\mu^+\mu^-$. Misidentification rates are minimal, with 0.1% for e^+e^- as $\mu^+\mu^-$, and 0.3% for $\mu^+\mu^-$ as e^+e^- , and pions are never misidentified as leptons (or vice versa).

To account for energy losses from bremsstrahlung in relativistic electrons (positrons), photons (satisfying the selection criteria described above) within a 0.05 rad cone around the electron's (positron's) initial momentum direction are identified, and their four-momenta are added to that of the electron (positron).

Signal candidates are reconstructed from a pair of oppositely charged pions, a lepton pair (either e^+e^- or $\mu^+\mu^-$), and two photons. A kinematic fit [50] enforces four-momentum conservation by constraining the total four-momentum of the final state particles to equal that of the initial e^+e^- collision. Backgrounds with incompatible final-states are suppressed by requiring $\chi^2/N_{\text{DOF}} < 25$, where χ^2 is the goodness-of-fit statistic of the kinematic fit, and $N_{\text{DOF}} = 4$ is the number of degrees of freedom in the fit. After this requirement, the average number of candidates per event is 1.1, with 94.5% of events yielding a single candidate. For the small fraction of events with multiple candidates, the candidate with the smallest χ^2/N_{DOF} is selected for further analysis.

The $\Upsilon(1S)$ state is reconstructed from the lepton pair in each signal candidate. MC simulations show similar $M(\ell^+\ell^-)$ invariant mass distributions for e^+e^- and $\mu^+\mu^-$ after the kinematic fit, allowing a unified selection window of [9.430, 9.499] GeV/ c^2 for both modes. This window encompasses $\pm 3\sigma$ around the $\Upsilon(1S)$ mass, with σ denoting the mass resolution derived from MC simulations.

The χ_{b1} and χ_{b2} states are reconstructed by combining the $\Upsilon(1S)$ with one of the two signal photons. The energy distributions of these two photons overlap significantly in the laboratory frame, complicating the assignment of each photon to its originating decay. However, in the $\Upsilon_J(1D)$ rest frame, energy resolution improves significantly, distinguishing the lower-energy photon (γ_L), from the $\Upsilon_J(1D) \rightarrow \gamma_L\chi_{b1}/\chi_{b2}$ decay, and the higher-energy photon (γ_H), from the $\chi_{b1}/\chi_{b2} \rightarrow \gamma_H\Upsilon(1S)$ decay. Simulations indicate that mis-reconstruction due to photon swapping occurs in less than 0.1% of cases, making its impact negligible.

The invariant mass $M[\gamma_H\Upsilon(1S)]$ of the χ_{b1}/χ_{b2} candidate is defined as:

$$M[\gamma_H\Upsilon(1S)] \equiv M(\gamma_H\ell^+\ell^-) - M(\ell^+\ell^-) + m[\Upsilon(1S)], \quad (3.1)$$

where $m[\Upsilon(1S)]$ is the nominal mass [4]. This subtracts the lepton pair mass and adds the known $\Upsilon(1S)$ mass, which enhances the resolution of the χ_{b1}/χ_{b2} mass peaks (7.9 MeV/ c^2). Signal windows are defined as [9.869, 9.915] GeV/ c^2 for χ_{b1} and [9.888, 9.934] GeV/ c^2 for χ_{b2} , corresponding to $\pm 3\sigma$ around their respective masses.

Analysis of simulated background samples (as described in Section 2) reveals a significant accumulation of events near $\cos(\theta_{\pi^+\pi^-}) = 1$, where $\theta_{\pi^+\pi^-}$ is the opening angle between the two pions in the laboratory frame. These events arise from radiative Bhabha ($e^+e^- \rightarrow e^+e^-\gamma$) and di-muon ($e^+e^- \rightarrow \mu^+\mu^-\gamma$) processes in which the emitted photon converts to an e^+e^- pair that have a small opening angle. When these converted e^+e^- pairs are misidentified as $\pi^+\pi^-$, they lead to the observed accumulation. To mitigate this background, we apply a requirement of $\cos(\theta_{\pi^+\pi^-}) < 0.95$. This cut eliminates essentially

100% of these background events while retaining 97% of the signal efficiency, as validated by MC simulations.

The process $e^+e^- \rightarrow \eta\Upsilon(2S)$, with a significant cross section near $\sqrt{s} = 10.75$ GeV [51], matches the final state studied in this analysis. MC simulations indicate that it produces a background peak in the key signal observable (the recoil mass against the $\pi^+\pi^-$ pair) near the $\Upsilon_J(1D)$ signal region, necessitating its careful removal. We apply a veto on the photon pair invariant mass, excluding events where $M(\gamma\gamma) \in [0.511, 0.576]$ GeV/ c^2 , corresponding to the η mass window. This criterion eliminates 99% of the $\eta\Upsilon(2S)$ background while preserving 85% of the signal efficiency, as determined from MC studies.

The primary remaining background after the event selection arises from $e^+e^- \rightarrow \omega\chi_{b1}/\chi_{b2}$, a well-studied process at Belle II [14]. This background, characterized by a broad distribution in the signal observable ($\pi^+\pi^-$ recoil mass), is modeled using MC simulations and incorporated into the fit as a fixed shape, as detailed in the subsequent section. Contributions from other background sources are found to be negligible.

4 Signal Extraction

To analyze the $\Upsilon_J(1D)$ spectrum, we have evaluated two methods: the invariant mass of the $\gamma\gamma\Upsilon(1S)$ system (after the kinematic fit) and the recoil mass against the $\pi^+\pi^-$ pair (prior to the kinematic fit). The recoil mass is defined as $M(\pi^+\pi^-)^{\text{recoil}} \equiv \sqrt{(P_{e^+e^-} - P_{\pi^+} - P_{\pi^-})^2}$, where $P_{e^+e^-}$ is the four-momentum of the e^+e^- collision system, and P_{π^+} and P_{π^-} are the four-momenta of the π^+ and π^- candidates, respectively. MC simulations reveal that the $\pi^+\pi^-$ recoil mass spectrum offers superior resolution (5.9 MeV/ c^2) compared to the $\gamma\gamma\Upsilon(1S)$ invariant mass spectrum (6.1 MeV/ c^2). This improvement stems from the Belle II detector's precise tracking capabilities for low-momentum charged pions (π^+ and π^-). Consequently, we adopt the $\pi^+\pi^-$ recoil mass spectrum for signal extraction to maximize sensitivity.

The $M(\pi^+\pi^-)^{\text{recoil}}$ distributions for signal MC samples, illustrating the expected shapes for $\Upsilon_2(1D)$, $\Upsilon_3(1D)$, and $\Upsilon(2S)$, are shown in Fig. 1, normalized to unit area for clarity. Figures 2 and 3 present the $M(\pi^+\pi^-)^{\text{recoil}}$ distributions for data events at each center-of-mass energy after applying all selection criteria, corresponding to the χ_{b1} and χ_{b2} channels, respectively. No significant $\Upsilon_J(1D)$ signal is observed at any of the collision energies studied. A small number of $\Upsilon(2S)$ events are observed at $\sqrt{s} = 10.745$ and 10.805 GeV, as expected, originating from the process $e^+e^- \rightarrow \pi^+\pi^-\Upsilon(2S)$. The measured cross sections for this process agree with prior Belle and Belle II results within uncertainties [11, 12, 52].

Signal yields are extracted via an unbinned extended maximum likelihood fit to each distribution. The fitted components are shown in Figs. 2 and 3. For the data sample at $\sqrt{s} = 10.701$ GeV which contains zero events, a binned fit with a 5 MeV bin width, where each bin (containing zero events) follows Poisson statistics, is employed instead. The probability density functions (PDFs) for the $\Upsilon(2S)$ and $\Upsilon_J(1D)$ signals are parameterized using shapes derived from their respective MC simulations (MC histograms). The yields for the $\Upsilon(2S)$ and $\Upsilon_J(1D)$ signals are allowed to float freely in the fit. To mitigate potential

anticorrelations arising from the small mass difference between the $\Upsilon_2(1D)$ and $\Upsilon_3(1D)$ states, we neglect cross-feed by fixing the contribution from the alternate state to zero. Specifically, for the χ_{b1} channel, we set the $\Upsilon_3(1D)$ yield to zero when extracting $\Upsilon_2(1D)$, and vice versa for the χ_{b2} channel. This approach ensures fit stability and yields more conservative upper limits. The background PDF consists of a constant term, with its yield allowed to float freely in the fit, and the $e^+e^- \rightarrow \omega\chi_{b1,b2}$ component. The $\omega\chi_{b1,b2}$ contribution, shaped from MC simulations and normalized to the cross sections reported in Ref. [14], is fixed during the fit. Notably, this background vanishes at $\sqrt{s} = 10.653$ and 10.701 GeV due to negligibly small production cross sections at these energies [14].

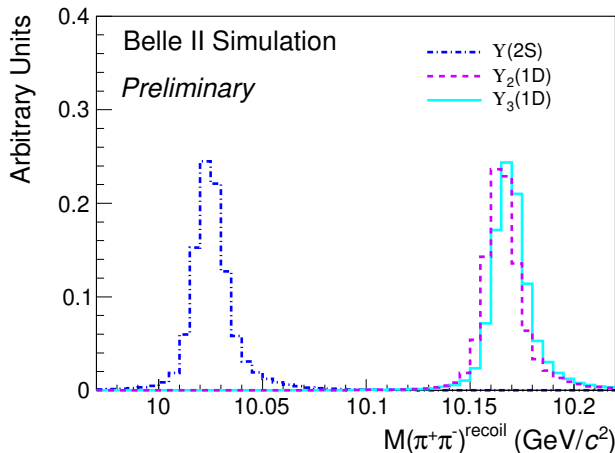


Figure 1. Normalized $M(\pi^+\pi^-)^{\text{recoil}}$ distributions for signal MC events. The dot-dashed blue line represents the $\Upsilon(2S)$ signal, the dashed violet line is the $\Upsilon_2(1D)$ signal, and the solid cyan line is the $\Upsilon_3(1D)$ signal.

5 Cross Section Measurement

Given the absence of a significant signal for $\Upsilon_J(1D)$ in the experimental data, we employ a Bayesian approach [4] to calculate the upper limit on the signal yield at 90% credibility for each center-of-mass energy. This method involves integrating the likelihood function over the signal yield parameter, ranging from zero to infinity, and determining the upper limit as the value where the cumulative probability reaches 90% of the total. By excluding negative signal yields, this approach ensures a conservative estimation. To account for systematic uncertainties, we convolve the likelihood function with a Gaussian function centered at each assumed signal yield, with the width of the Gaussian corresponding to the total systematic uncertainty.

At each center-of-mass energy, the upper limit on the signal yield of $\Upsilon_J(1D)$ is subsequently converted into an upper limit on the product of the dressed cross section and branching fraction for the specific decay channels $e^+e^- \rightarrow \pi^+\pi^-\Upsilon_2(1D)$ with $\Upsilon_2(1D) \rightarrow \gamma\chi_{b1}$, and $e^+e^- \rightarrow \pi^+\pi^-\Upsilon_3(1D)$ with $\Upsilon_3(1D) \rightarrow \gamma\chi_{b2}$. The calculation is performed using

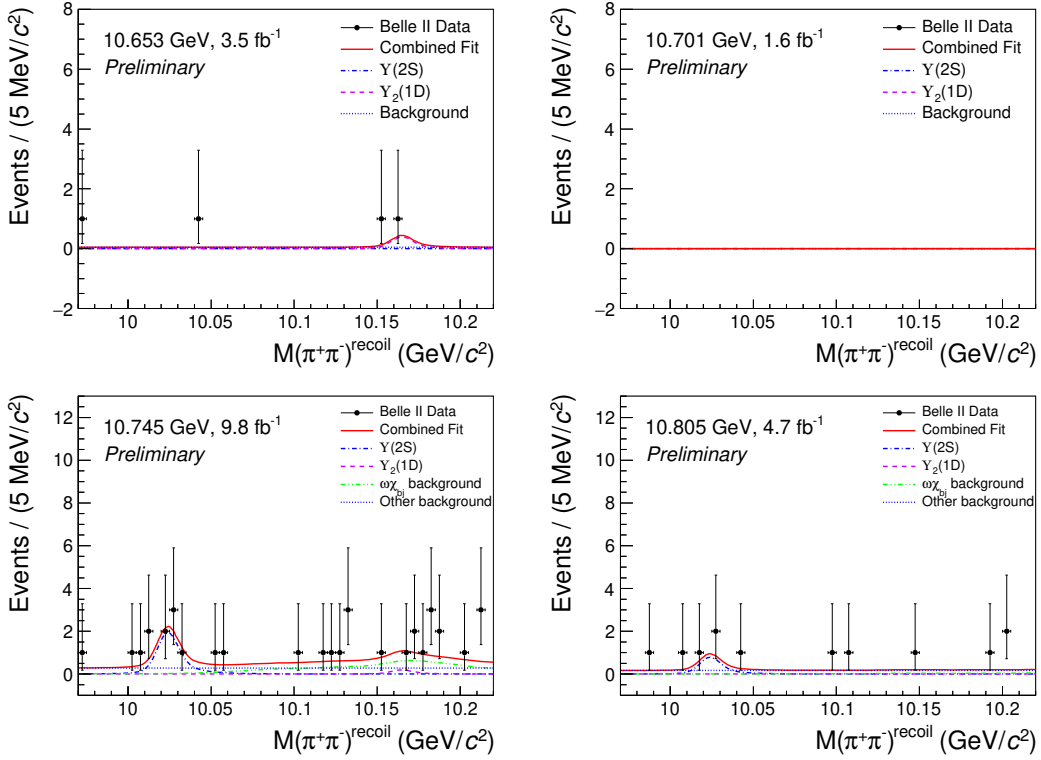


Figure 2. Fits to the $M(\pi^+\pi^-)^{\text{recoil}}$ distributions for data events in the χ_{b1} channel. Dots with error bars represent the data, the solid red line is the total fit, the dashed violet line is the $\Upsilon_2(1D)$ signal component, the dot-dashed blue line is the $\Upsilon(2S)$ signal component, the double-dot-dashed green line represents the $\omega_{\chi_{b1,b2}}$ background, and the dotted blue line is the constant background component. Note that the $\sqrt{s} = 10.701$ GeV sample contains zero events.

the following expression:

$$\begin{aligned} & \sigma[e^+e^- \rightarrow \pi^+\pi^-\Upsilon_2(1D)] \times \mathcal{B}[\Upsilon_2(1D) \rightarrow \gamma\chi_{b1}] \\ &= \frac{N_{\Upsilon_2(1D)}(1 - R_{\chi_{b2}})}{\mathcal{L}\mathcal{B}[\chi_{b1} \rightarrow \gamma\Upsilon(1S)]\mathcal{B}[\Upsilon(1S) \rightarrow \ell^+\ell^-]e^w(1 + \delta)}, \end{aligned} \quad (5.1)$$

and

$$\begin{aligned} & \sigma[e^+e^- \rightarrow \pi^+\pi^-\Upsilon_3(1D)] \times \mathcal{B}[\Upsilon_3(1D) \rightarrow \gamma\chi_{b2}] \\ &= \frac{N_{\Upsilon_3(1D)}}{\mathcal{L}\mathcal{B}[\chi_{b2} \rightarrow \gamma\Upsilon(1S)]\mathcal{B}[\Upsilon(1S) \rightarrow \ell^+\ell^-]e^w(1 + \delta)}. \end{aligned} \quad (5.2)$$

Here, $N_{\Upsilon_J(1D)}$ represents the upper limit on the number of signal events for the respective $\Upsilon_J(1D)$ channel, \mathcal{L} is the integrated luminosity, and \mathcal{B} denotes the relevant branching fractions. MC simulations reveal an overlap between the χ_{b1} and χ_{b2} peaks, resulting in potential cross-contamination between them. For the $\Upsilon_2(1D)$ channel, the contamination from the $\Upsilon_2(1D) \rightarrow \gamma\chi_{b2}$ decay is quantified by the ratio $R_{\chi_{b2}}$, which is computed based on the selection efficiencies of the χ_{b1} and χ_{b2} channels and the theoretically predicted branching ratios for $\Upsilon_2(1D) \rightarrow \gamma\chi_{b1}$ and $\Upsilon_2(1D) \rightarrow \gamma\chi_{b2}$ [9]. Conversely, for the $\Upsilon_3(1D)$

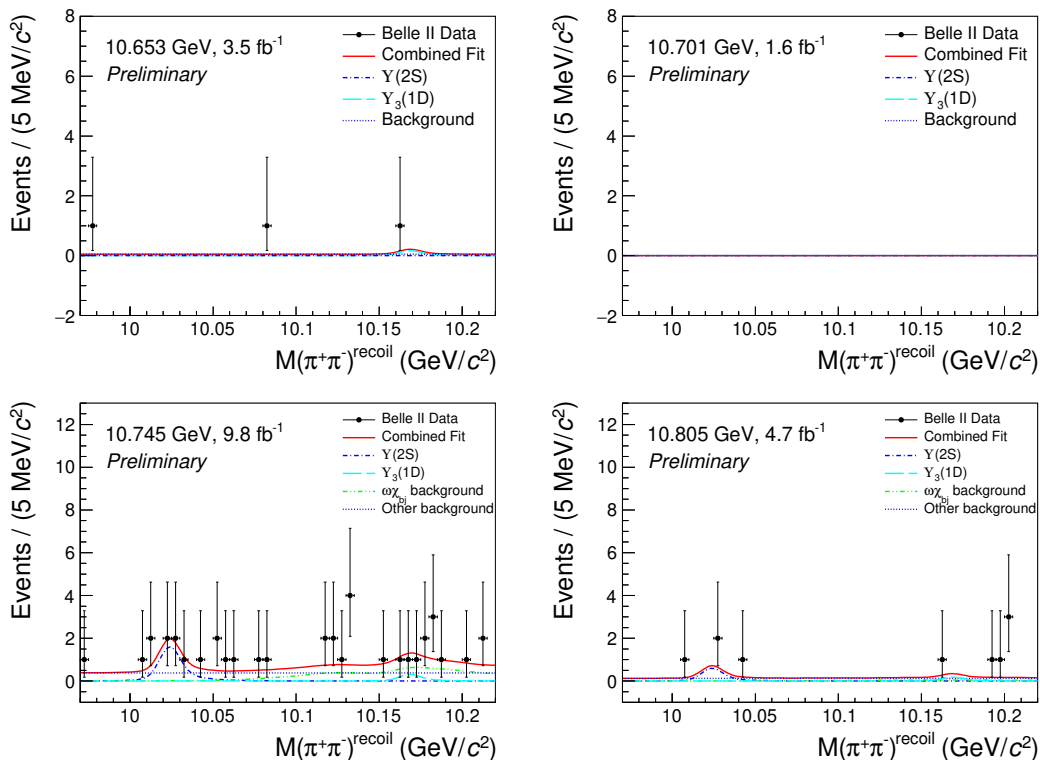


Figure 3. Fits to the $M(\pi^+\pi^-)^{\text{recoil}}$ distributions for data events in the χ_{b2} channel. Dots with error bars represent the data, the solid red line is the total fit, the long-dashed cyan line is the $\Upsilon_3(1D)$ signal component, the dot-dashed blue line is the $\Upsilon(2S)$ signal component, the double-dot-dashed green line represents the $\omega_{\chi_{b1,b2}}$ background, and the dotted blue line is the constant background component. Note that the $\sqrt{s} = 10.701$ GeV sample contains zero events.

channel, the contamination from $\Upsilon_3(1D) \rightarrow \gamma\chi_{b1}$ is negligible, as the branching fraction for this decay is predicted to be nearly zero according to theoretical calculations [9].

The re-weighted reconstruction efficiency, ϵ^w , is obtained by adjusting the $\frac{1}{s}$ cross section line-shape used in the MC generation to match the $\Upsilon(10753)$ resonance line-shape, following the methodology outlined in Refs. [12, 53]. The radiative correction factor, $(1+\delta)$, is defined as:

$$(1 + \delta) = \frac{\int_0^{x_m} \sigma^{\text{dress}}(s(1-x))W(x,s) dx}{\sigma^{\text{dress}}(s)}, \quad (5.3)$$

where $\sigma^{\text{dress}}(s)$ is the energy-dependent dressed cross section modeled using the $\Upsilon(10753)$ resonance line-shape. The radiator function $W(x,s)$ accounts for ISR effects, as described in Ref. [54]. The upper integration limit, $x_m = 1 - s_m/s$, represents the maximum fraction of energy carried by the ISR photon, with $s_m = [m(\pi^+) + m(\pi^-) + m[\Upsilon_J(1D)]]^2$ being the minimum energy squared required to produce the final state.

Tables 1 and 2 present the measurements of $\sigma[e^+e^- \rightarrow \pi^+\pi^-\Upsilon_2(1D)] \times \mathcal{B}[\Upsilon_2(1D) \rightarrow \gamma\chi_{b1}]$ and $\sigma[e^+e^- \rightarrow \pi^+\pi^-\Upsilon_3(1D)] \times \mathcal{B}[\Upsilon_3(1D) \rightarrow \gamma\chi_{b2}]$, respectively, assuming the $\Upsilon(10753)$ resonance line-shape hypothesis for the cross section. To offer an alternative

Table 1. Measurements on the product of the dressed cross section and branching fraction, $\sigma[e^+e^- \rightarrow \pi^+\pi^-\Upsilon_2(1D)] \times \mathcal{B}[\Upsilon_2(1D) \rightarrow \gamma\chi_{b1}]$, at various center-of-mass energies \sqrt{s} . Parameters include integrated luminosity \mathcal{L} , re-weighted efficiency ϵ^w , radiative correction factor $(1 + \delta)$, signal yield $N_{\Upsilon_2(1D)}$, contamination ratio $R_{\chi_{b2}}$, and the resulting product $\sigma \times \mathcal{B}$ (incorporating systematic uncertainties), estimated under the $\Upsilon(10753)$ line-shape hypothesis for the cross section. Values in the parentheses are for the $\Upsilon(5S)$ line-shape hypothesis.

\sqrt{s} (GeV)	\mathcal{L} (fb $^{-1}$)	ϵ^w	$(1 + \delta)$	$N_{\Upsilon_2(1D)}$	$R_{\chi_{b2}}$	$\sigma \times \mathcal{B}$ (pb)
10.653	3.5	0.180 (0.172)	0.895 (0.819)	< 4.6	0.099	< 0.43 (< 0.49)
10.701	1.6	0.202 (0.177)	0.723 (0.923)	< 2.3	0.100	< 0.52 (< 0.46)
10.745	9.8	0.215 (0.191)	0.587 (0.885)	< 6.8	0.099	< 0.29 (< 0.21)
10.805	4.7	0.176 (0.216)	1.039 (0.732)	< 3.0	0.100	< 0.18 (< 0.21)

Table 2. Measurements on the product of the dressed cross section and branching fraction, $\sigma[e^+e^- \rightarrow \pi^+\pi^-\Upsilon_3(1D)] \times \mathcal{B}[\Upsilon_3(1D) \rightarrow \gamma\chi_{b2}]$, at various center-of-mass energies \sqrt{s} . Parameters include integrated luminosity \mathcal{L} , re-weighted efficiency ϵ^w , radiative correction factor $(1 + \delta)$, signal yield $N_{\Upsilon_3(1D)}$, and the resulting product $\sigma \times \mathcal{B}$ (incorporating systematic uncertainties), estimated under the $\Upsilon(10753)$ line-shape hypothesis for the cross section. Values in the parentheses are for the $\Upsilon(5S)$ line-shape hypothesis.

\sqrt{s} (GeV)	\mathcal{L} (fb $^{-1}$)	ϵ^w	$(1 + \delta)$	$N_{\Upsilon_3(1D)}$	$\sigma \times \mathcal{B}$ (pb)
10.653	3.5	0.177 (0.169)	0.893 (0.827)	< 3.6	< 0.73 (< 0.83)
10.701	1.6	0.202 (0.180)	0.724 (0.901)	< 2.3	< 1.12 (< 1.01)
10.745	9.8	0.212 (0.194)	0.587 (0.883)	< 7.4	< 0.69 (< 0.53)
10.805	4.7	0.170 (0.209)	1.042 (0.728)	< 5.2	< 0.71 (< 0.83)

perspective, the same tables include values in parentheses, corresponding to estimates derived under the $\Upsilon(5S)$ resonance hypothesis, where the radiative correction factor $(1 + \delta)$ and the efficiency ϵ^w are recalculated to reflect the $\Upsilon(5S)$ line-shape. It is noteworthy that the center-of-mass energies of the data samples in this analysis ($\sqrt{s} = 10.653, 10.701, 10.745, \text{ and } 10.805$ GeV) lie well below the $\Upsilon(5S)$ peak, where its contribution is expected to be minimal, in contrast to the $\Upsilon(10753)$ resonance, where these energies cover the peak region of the resonance.

6 Systematic Uncertainty

The systematic uncertainties in the cross section measurement stem from several sources. These include uncertainties in integrated luminosity, trigger simulation, tracking efficiency, photon detection efficiency, branching fractions, decay model, MC statistics, signal parameterization, and background modeling. Each contributing factor is elaborated below.

The integrated luminosity at Belle II is determined with a precision of 0.6% using Bhabha, di-photon and di-muon events, as documented in Ref. [55]. The systematic un-

certainty associated with the trigger simulation is conservatively evaluated at 1.0%. This estimate is based on discrepancies in trigger efficiencies between data (99.9%) and MC simulations (99.3%), analyzed through the $e^+e^- \rightarrow 2(\pi^+\pi^-\pi^0)$ control sample. The reconstruction efficiency of a single high-momentum charged track ($p > 0.2$ GeV/ c) carries a systematic uncertainty of 0.3%, derived from tracking efficiency comparisons between data and MC using τ -pair events; for the two high-momentum leptons in the signal, this yields a total uncertainty of 0.6%. For pion tracks, the reconstruction efficiency uncertainty is 0.3% per track at high momentum ($p > 0.2$ GeV/ c), while efficiencies for low-momentum pions ($p < 0.2$ GeV/ c) in the signal MC are reweighted to match data based on studies of $B^0 \rightarrow D^{*-}\pi^+$ decays; the combined uncertainty for the pion tracks is estimated at 0.9%. Photon detection efficiencies in the signal MC are adjusted to align with data, using measurements from the process $e^+e^- \rightarrow \mu^+\mu^-\gamma_{\text{ISR}}$, and have an associated uncertainty of 3.6%.

The branching fractions $\mathcal{B}[\chi_{b1} \rightarrow \gamma\Upsilon(1S)]$, $\mathcal{B}[\chi_{b2} \rightarrow \gamma\Upsilon(1S)]$, $\mathcal{B}[\Upsilon(1S) \rightarrow e^+e^-]$, and $\mathcal{B}[\Upsilon(1S) \rightarrow \mu^+\mu^-]$ have uncertainties of 5.7%, 5.6%, 3.3%, and 1.6% [4], respectively. The combined systematic uncertainties for the product $\mathcal{B}[\chi_{bJ'} \rightarrow \gamma\Upsilon(1S)]\mathcal{B}[\Upsilon(1S) \rightarrow \ell^+\ell^-]$ are computed as 6.3% and 6.3%, for $J' = 1$ and $J' = 2$, respectively.

The default signal MC simulation employs a three-body PHSP model for $\pi^+\pi^-\Upsilon_J(1D)$ production, ensuring a model-independent description. To evaluate the systematic uncertainty associated with the $\pi^+\pi^-$ dynamics, an alternative model incorporating the scalar resonance $f_0(500)$ ($J^{PC} = 0^{++}$) is used. This yields a relative efficiency difference of 3.6%, which is assigned as the systematic uncertainty for the decay model. The estimate also accounts for effects from the γ -conversion background veto applied to $\cos(\theta_{\pi^+\pi^-})$.

The systematic uncertainty due to the size of the MC sample is determined using the expression $\sqrt{\frac{\epsilon(1-\epsilon)}{N}}/\epsilon$, where ϵ represents the signal reconstruction efficiency and N is the number of generated MC events. This uncertainty is estimated to be 0.4%.

Direct comparisons of fits to data can be significantly affected by statistical fluctuations, potentially masking true systematic effects. To address this, we conduct a MC pseudo-experiment study to quantify the systematic uncertainty associated with signal parameterization. We generate 2000 MC pseudo-experiment samples using the default signal PDF, derived from the signal MC shape. Each sample is fitted with two signal models: the default signal PDF and an alternative model defined as a Crystal Ball function [56]. To account for possible differences in resolution between data and MC simulation, the resolution parameter of the Crystal Ball function is first adjusted to match the signal MC shape and then varied within ± 2.2 MeV. This ± 2.2 MeV range corresponds to the measured uncertainty on the data-MC resolution difference obtained from the control sample $e^+e^- \rightarrow \pi^+\pi^-\Upsilon(2S)[\rightarrow \ell^+\ell^-]$ [12], where the resolution differs by 0.1 ± 2.2 MeV. The resulting relative difference in fitted signal yield between the two models is 0.5%, which is assigned as the systematic uncertainty due to signal parameterization.

We assess the systematic uncertainty associated with the background modeling using a similar MC pseudo-experiment approach. We generate 2000 MC pseudo-experiment samples, each containing signal and background events. The signal is modeled with the

default signal PDF, while the background is modeled with the default 0th-order polynomial (constant term). Each sample is fitted with two background models: the default model and an alternative model defined as a first-order polynomial. By comparing the signal yield distributions from the two fits, we estimate the impact of varying the background PDF shape. The relative difference in signal yield is calculated to be 0.2%, which is assigned as the systematic uncertainty due to the background shape.

The radiative correction in e^+e^- collisions depends on the line-shape of the cross section for the process $e^+e^- \rightarrow \pi^+\pi^-\Upsilon_J(1D)$. Due to uncertainty in the exact line-shape, we refrain from assigning a systematic uncertainty to the radiative correction. Instead, we adopt an approach where the cross section is evaluated under two distinct hypotheses, as mentioned earlier: one assuming it follows the $\Upsilon(10753)$ resonance line-shape, and another assuming the $\Upsilon(5S)$ resonance line-shape. Results based on both hypotheses are reported in Tables 1 and 2.

The systematic uncertainty from the $\Upsilon(1S)$ signal window on the $M(\ell^+\ell^-)$ invariant mass is negligible, due to the accurate modeling of lepton resolution in the MC. This is supported by lepton performance studies using τ -pair events, as well as resolution investigations in the control sample $e^+e^- \rightarrow \pi^+\pi^-\Upsilon(2S) \rightarrow \pi^+\pi^-\ell^+\ell^-$ [12]. The systematic uncertainty from the $\chi_{b1,b2}$ signal window on the $M[\gamma_H\Upsilon(1S)]$ invariant mass is negligible due to the photon energy corrections applied to the MC simulation to match experimental data, using the $\pi^0 \rightarrow \gamma\gamma$ sample. The systematic uncertainty from the η background veto on $M(\gamma_L\gamma_H)$ invariant mass is negligible, as it is mitigated by the same photon energy corrections.

Assuming all systematic uncertainty sources are independent, the total systematic uncertainty is obtained by combining them in quadrature, resulting in a value of 8.3%. A summary of the systematic uncertainties is presented in Table 3.

Table 3. Systematic uncertainties for the measurement of $\sigma[e^+e^- \rightarrow \pi^+\pi^-\Upsilon_J(1D)] \times \mathcal{B}[\Upsilon_J(1D) \rightarrow \gamma\chi_{bJ}]$.

Source	Uncertainty (%)
Integrated luminosity	0.6
Trigger simulation	1.0
Lepton efficiency	0.6
Pion efficiency	0.9
Photon efficiency	3.6
Branching fractions	6.3
Decay model	3.6
MC sample size	0.4
Signal parameterization	0.5
Background shape	0.2
Quadrature sum	8.3

The systematic uncertainty associated with the fixed background from $e^+e^- \rightarrow \omega\chi_{b1,b2}$

in the signal extraction is evaluated by varying its normalization by $\pm 24\%$, corresponding to the combined statistical and systematic uncertainty reported in Ref. [14]. For each variation, the upper limit on the $\Upsilon_J(1D)$ signal yield is recalculated, and the most conservative value, i.e. the largest upper limit obtained from the nominal and varied background scenarios, is adopted as the final result. This adjustment increases the upper limits on the $\Upsilon_J(1D)$ signal yields by 0 to 0.7 events across different center-of-mass energies, depending on the contribution from $e^+e^- \rightarrow \omega\chi_{b1,b2}$.

7 Discussion

In an inclusive analysis of $\Upsilon(5S) \rightarrow \pi^+\pi^-X$ decays at Belle [10], the yields derived from fits to the dipion missing mass spectrum are $(143.8 \pm 8.7 \pm 6.8) \times 10^3$ and $(22.4 \pm 7.8) \times 10^3$ for $\Upsilon(2S)$ and $\Upsilon_J(1D)$, respectively. Utilizing the cross section for $e^+e^- \rightarrow \pi^+\pi^-\Upsilon(2S)$ at 10.866 GeV, measured as 4.07 ± 0.18 pb in Ref. [11] with the same data sample, we estimate the cross section for $e^+e^- \rightarrow \pi^+\pi^-\Upsilon_2(1D)$ to be 0.63 ± 0.22 pb at this energy. This estimation assumes comparable reconstruction efficiencies between $\Upsilon(2S)$ and $\Upsilon_J(1D)$ and attributes the observed $\Upsilon_J(1D)$ signal predominantly to the $\Upsilon_2(1D)$ state, consistent with the conclusive identification of the 1^3D_2 configuration by the CLEO [7] and BaBar [8] collaborations, which reported inconclusive evidence for other J states. Incorporating the theoretical branching fraction for $\Upsilon_2(1D) \rightarrow \gamma\chi_{b1}$, estimated at approximately 0.73 [9] and supported by additional theoretical calculations [57–59], we derive the product of the cross section and branching fraction, $\sigma[e^+e^- \rightarrow \pi^+\pi^-\Upsilon_2(1D)] \times \mathcal{B}(\Upsilon_2(1D) \rightarrow \gamma\chi_{b1})$, to be approximately 0.46 ± 0.16 pb at $\sqrt{s} = 10.866$ GeV. Starting from this estimated value, we extrapolate the energy-dependent $\sigma[e^+e^- \rightarrow \pi^+\pi^-\Upsilon_2(1D)] \times \mathcal{B}(\Upsilon_2(1D) \rightarrow \gamma\chi_{b1})$ under two distinct hypotheses: production from the $\Upsilon(10753)$ resonance and production from the $\Upsilon(5S)$ resonance. These extrapolated cross sections are illustrated in Fig. 4, with the left panel depicting the $\Upsilon(10753)$ hypothesis and the right panel the $\Upsilon(5S)$ hypothesis. The figure also includes our measured 90% credible upper limits (as listed in Table 1), represented by inverted triangles. A direct comparison reveals that the $\pi^+\pi^-\Upsilon_J(1D)$ system is more consistent with production from the $\Upsilon(5S)$ resonance, as the measured upper limits are well above the expected values, essentially null, under this hypothesis (Fig. 4, right panel). Conversely, at $\sqrt{s} = 10.745$ GeV, near the $\Upsilon(10753)$ peak, the upper limits fall significantly below the anticipated cross section (Fig. 4, left panel), indicating a pronounced suppression in the coupling of the $\Upsilon(10753)$ resonance to $\Upsilon_J(1D)$ states via dipion transitions. This suppression, when considered alongside the $\Upsilon(5S)$ resonance, contributes to the elucidation of the $\Upsilon(10753)$'s intrinsic nature.

8 Summary

We present a comprehensive study of the processes $e^+e^- \rightarrow \pi^+\pi^-\Upsilon_J(1D)$, where $J = 2$ or 3, utilizing a 19.6 fb^{-1} data sample collected by the Belle II detector at the SuperKEKB e^+e^- asymmetric-energy collider. The data were acquired at center-of-mass energies of $\sqrt{s} = 10.653, 10.701, 10.745,$ and 10.805 GeV, strategically chosen to probe the $\Upsilon(10753)$

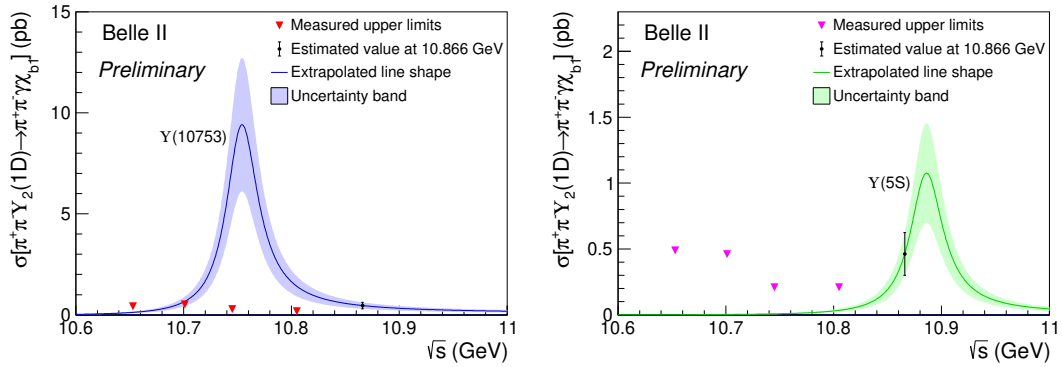


Figure 4. Measured 90% credible upper limits on the product $\sigma[e^+e^- \rightarrow \pi^+\pi^-\Upsilon_2(1D)] \times \mathcal{B}(\Upsilon_2(1D) \rightarrow \gamma\chi_{b1})$ as a function of center-of-mass energy, evaluated under the $\Upsilon(10753)$ resonance hypothesis (left) and the $\Upsilon(5S)$ resonance hypothesis (right). Inverted triangles denote the measured upper limits. The dark dots with error bars indicate the estimated value at 10.866 GeV, derived from Belle results [10]. The solid curves represent the extrapolated cross sections under the respective resonance hypotheses, with the filled bands illustrating the uncertainties associated with these extrapolations.

resonance. For each center-of-mass energy, upper limits at 90% credibility on the products of the cross sections and branching fractions, $\sigma[e^+e^- \rightarrow \pi^+\pi^-\Upsilon_2(1D)] \times \mathcal{B}(\Upsilon_2(1D) \rightarrow \gamma\chi_{b1})$ and $\sigma[e^+e^- \rightarrow \pi^+\pi^-\Upsilon_3(1D)] \times \mathcal{B}(\Upsilon_3(1D) \rightarrow \gamma\chi_{b2})$, are determined and reported.

Acknowledgments

This work, based on data collected using the Belle II detector, which was built and commissioned prior to March 2019, was supported by Higher Education and Science Committee of the Republic of Armenia Grant No. 23LCG-1C011; Australian Research Council and Research Grants No. DP200101792, No. DP210101900, No. DP210102831, No. DE220100462, No. LE210100098, and No. LE230100085; Austrian Federal Ministry of Education, Science and Research, Austrian Science Fund (FWF) Grants DOI: 10.55776/P34529, DOI: 10.55776/J4731, DOI: 10.55776/J4625, DOI: 10.55776/M3153, and DOI: 10.55776/PAT1836324, and Horizon 2020 ERC Starting Grant No. 947006 “InterLeptons”; Natural Sciences and Engineering Research Council of Canada, Digital Research Alliance of Canada, and Canada Foundation for Innovation; National Key R&D Program of China under Contract No. 2024YFA1610503, and No. 2024YFA1610504 National Natural Science Foundation of China and Research Grants No. 11575017, No. 11761141009, No. 11705209, No. 11975076, No. 12135005, No. 12150004, No. 12161141008, No. 12405099, No. 12475093, and No. 12175041, Shandong Provincial Natural Science Foundation Project ZR2022JQ02, and Shandong Postdoctoral Science Foundation under Contract No. SDCX-ZG-202400324; the Czech Science Foundation Grant No. 22-18469S, Regional funds of EU/MEYS: OPJAK FORTE CZ.02.01.01/00/22.008/0004632 and Charles University Grant Agency project No. 246122; European Research Council, Seventh Framework PIF-GA-2013-622527, Horizon 2020 ERC-Advanced Grants No. 267104 and No. 884719, Horizon 2020 ERC-Consolidator Grant No. 819127, Horizon 2020 Marie

Sklodowska-Curie Grant Agreement No. 700525 “NIOBE” and No. 101026516, and Horizon Europe Marie Sklodowska-Curie Staff Exchange project JENNIFER3 Grant Agreement No. 101183137 (European grants); L’Institut National de Physique Nucléaire et de Physique des Particules (IN2P3) du CNRS under Project Identification No. CNRS-IN2P3-14-PP-033 and L’Agence Nationale de la Recherche (ANR) under Grant No. ANR-23-CE31-0018 and ANR-25-CE31-1333 (France); BMFTR, DFG, HGF, MPG, and AvH Foundation (Germany); Department of Atomic Energy under Project Identification No. RTI 4002, Department of Science and Technology, and UPES SEED funding programs No. UPES/R&D-SEED-INFRA/17052023/01 and No. UPES/R&D-SOE/20062022/06 (India); Israel Science Foundation Grant No. 2476/17, U.S.-Israel Binational Science Foundation Grant No. 2016113, and Israel Ministry of Science Grant No. 3-16543; Istituto Nazionale di Fisica Nucleare and the Research Grants BELLE2, and the ICSC – Centro Nazionale di Ricerca in High Performance Computing, Big Data and Quantum Computing, funded by European Union – NextGenerationEU; Japan Society for the Promotion of Science, Grant-in-Aid for Scientific Research Grants No. 16H03968, No. 16H03993, No. 16H06492, No. 16K05323, No. 17H01133, No. 17H05405, No. 18K03621, No. 18H03710, No. 18H05226, No. 19H00682, No. 20H05850, No. 20H05858, No. 22H00144, No. 22K14056, No. 22K21347, No. 23H05433, No. 26220706, and No. 26400255, and the Ministry of Education, Culture, Sports, Science, and Technology (MEXT) of Japan; National Research Foundation (NRF) of Korea Grants No. 2021R1-A6A1A-03043957, No. 2021R1-F1A-1064008, No. 2022R1-A2C-1003993, No. 2022R1-A2C-1092335, No. RS-2016-NR017151, No. RS-2018-NR031074, No. RS-2021-NR060129, No. RS-2023-00208693, No. RS-2024-00354342 and No. RS-2025-02219521, Radiation Science Research Institute, Foreign Large-Size Research Facility Application Supporting project, the Global Science Experimental Data Hub Center, the Korea Institute of Science and Technology Information (K25L2M2C3) and KREONET/GLORIAD; Universiti Malaya RU grant, Akademi Sains Malaysia, and Ministry of Education Malaysia; Frontiers of Science Program Contracts No. FOINS-296, No. CB-221329, No. CB-236394, No. CB-254409, and No. CB-180023, and SEP-CINVESTAV Research Grant No. 237 (Mexico); the Polish Ministry of Science and Higher Education and the National Science Center; the Ministry of Science and Higher Education of the Russian Federation and the HSE University Basic Research Program, Moscow; University of Tabuk Research Grants No. S-0256-1438 and No. S-0280-1439 (Saudi Arabia), and Researchers Supporting Project number (RSPD2025R873), King Saud University, Riyadh, Saudi Arabia; Slovenian Research Agency and Research Grants No. J1-50010 and No. P1-0135; Ikerbasque, Basque Foundation for Science, State Agency for Research of the Spanish Ministry of Science and Innovation through Grant No. PID2022-136510NB-C33, Spain, Agencia Estatal de Investigación, Spain Grant No. RYC2020-029875-I and Generalitat Valenciana, Spain Grant No. CIDEGENT/2018/020; The Knut and Alice Wallenberg Foundation (Sweden), Contracts No. 2021.0174, No. 2021.0299, and No. 2023.0315; National Science and Technology Council, and Ministry of Education (Taiwan); Thailand Center of Excellence in Physics; TUBITAK ULAKBIM (Turkey); National Research Foundation of Ukraine, Project No. 2020.02/0257, and Ministry of Education and Science of Ukraine; the U.S. National Science Foundation and Research Grants No. PHY-

1913789 and No. PHY-2111604, and the U.S. Department of Energy and Research Awards No. DE-AC06-76RLO1830, No. DE-SC0007983, No. DE-SC0009824, No. DE-SC0009973, No. DE-SC0010007, No. DE-SC0010073, No. DE-SC0010118, No. DE-SC0010504, No. DE-SC0011784, No. DE-SC0012704, No. DE-SC0019230, No. DE-SC0021616, No. DE-SC0022350, No. DE-SC0023470; and the Vietnam Academy of Science and Technology (VAST) under Grants No. NVCC.05.02/25-25 and No. DL0000.05/26-27.

These acknowledgements are not to be interpreted as an endorsement of any statement made by any of our institutes, funding agencies, governments, or their representatives.

We thank the SuperKEKB team for delivering high-luminosity collisions; the KEK cryogenics group for the efficient operation of the detector solenoid magnet and IBelle on site; the KEK Computer Research Center for on-site computing support; the NII for SINET6 network support; and the raw-data centers hosted by BNL, DESY, GridKa, IN2P3, INFN, and the University of Victoria.

References

- [1] N. Brambilla et al., *Heavy Quarkonium: Progress, Puzzles, and Opportunities*, *Eur. Phys. J. C* **71** (2011) 1534 [[1010.5827](#)].
- [2] S. Godfrey and N. Isgur, *Mesons in a Relativized Quark Model with Chromodynamics*, *Phys. Rev. D* **32** (1985) 189.
- [3] E. Eichten, K. Gottfried, T. Kinoshita, K.D. Lane and T.-M. Yan, *Charmonium: The Model*, *Phys. Rev. D* **17** (1978) 3090.
- [4] PARTICLE DATA GROUP collaboration, *Review of Particle Physics*, *PTEP* **2022** (2022) 083C01.
- [5] C. Patrignani, T.K. Pedlar and J.L. Rosner, *Recent Results in Bottomonium*, *Ann. Rev. Nucl. Part. Sci.* **63** (2012) 2008 [[1212.6552](#)].
- [6] E. Eichten, S. Godfrey, H. Mahlke and J.L. Rosner, *Quarkonia and their transitions*, *Rev. Mod. Phys.* **80** (2008) 1161 [[hep-ph/0701208](#)].
- [7] CLEO collaboration, *First observation of a Upsilon(1D) state*, *Phys. Rev. D* **70** (2004) 032001 [[hep-ex/0404021](#)].
- [8] BABAR collaboration, *Observation of the $\Upsilon(1^3D_J)$ Bottomonium State through Decays to $\pi^+\pi^-\Upsilon(1S)$* , *Phys. Rev. D* **82** (2010) 111102 [[1004.0175](#)].
- [9] W.J. Deng, H. Liu, L.C. Gui and X.H. Zhong, *Spectrum and electromagnetic transitions of bottomonium*, *Phys. Rev. D* **95** (2017) 074002 [[1607.04696](#)].
- [10] BELLE collaboration, *First observation of the P-wave spin-singlet bottomonium states $h_b(1P)$ and $h_b(2P)$* , *Phys. Rev. Lett.* **108** (2012) 032001 [[1103.3419](#)].
- [11] BELLE collaboration, *Observation of a new structure near 10.75 GeV in the energy dependence of the $e^+e^- \rightarrow \Upsilon(nS)\pi^+\pi^-$ ($n = 1, 2, 3$) cross sections*, *JHEP* **10** (2019) 220 [[1905.05521](#)].
- [12] BELLE II collaboration, *Study of $\Upsilon(10753)$ decays to $\pi^+\pi^-\Upsilon(nS)$ final states at Belle II*, *JHEP* **07** (2024) 116 [[2401.12021](#)].

- [13] BELLE II collaboration, *Observation of $e^+e^- \rightarrow \eta\Upsilon(2S)$ and search for $e^+e^- \rightarrow \eta\Upsilon(1S), \gamma X_b$ at \sqrt{s} near 10.75 GeV*, [2509.01917](#).
- [14] BELLE II collaboration, *Observation of $e^+e^- \rightarrow \omega\chi_{bJ}(1P)$ and search for $X_b \rightarrow \omega\Upsilon(1S)$ at \sqrt{s} near 10.75 GeV*, *Phys. Rev. Lett.* **130** (2023) 091902 [[2208.13189](#)].
- [15] BELLE AND BELLE II collaboration, *Improved measurement of Born cross sections for $\chi_{bJ}\omega$ and $\chi_{bJ}(\pi^+\pi^-\pi^0)_{\text{non-}\omega}$ ($J = 0, 1, 2$) at Belle and Belle II*, [2510.25461](#).
- [16] BELLE collaboration, *Observation of $e^+e^- \rightarrow \pi^+\pi^-\pi^0\chi_{bJ}$ and Search for $X_b \rightarrow \omega\Upsilon(1S)$ at $\sqrt{s} = 10.867$ GeV*, *Phys. Rev. Lett.* **113** (2014) 142001 [[1408.0504](#)].
- [17] Z.Y. Bai, Y.S. Li, Q. Huang, X. Liu and T. Matsuki, *$\Upsilon(10753) \rightarrow \Upsilon(nS)\pi^+\pi^-$ decays induced by hadronic loop mechanism*, *Phys. Rev. D* **105** (2022) 074007 [[2201.12715](#)].
- [18] Y.S. Li, Z.Y. Bai, Q. Huang and X. Liu, *Hidden-bottom hadronic decays of $\Upsilon(10753)$ with a $\eta^{(\prime)}$ or ω emission*, *Phys. Rev. D* **104** (2021) 034036 [[2106.14123](#)].
- [19] Q. Li, M.S. Liu, Q.F. Lü, L.C. Gui and X.H. Zhong, *Canonical interpretation of $Y(10750)$ and $Y(10860)$ in the Υ family*, *Eur. Phys. J. C* **80** (2020) 59 [[1905.10344](#)].
- [20] B. Chen, A. Zhang and J. He, *Bottomonium spectrum in the relativistic flux tube model*, *Phys. Rev. D* **101** (2020) 014020 [[1910.06065](#)].
- [21] J.F. Giron and R.F. Lebed, *Spectrum of the hidden-bottom and the hidden-charm-strange exotics in the dynamical diquark model*, *Phys. Rev. D* **102** (2020) 014036 [[2005.07100](#)].
- [22] V. Kher, R. Chaturvedi, N. Devlani and A.K. Rai, *Bottomonium spectroscopy using Coulomb plus linear (Cornell) potential*, *Eur. Phys. J. Plus* **137** (2022) 357 [[2201.08317](#)].
- [23] Y.S. Li, Z.Y. Bai and X. Liu, *Investigating the $\Upsilon(10753) \rightarrow \Upsilon(1^3D_J)\eta$ transitions*, *Phys. Rev. D* **105** (2022) 114041 [[2205.04049](#)].
- [24] W.H. Liang, N. Ikeno and E. Oset, *$\Upsilon(nl)$ decay into $B^{(*)}\bar{B}^{(*)}$* , *Phys. Lett. B* **803** (2020) 135340 [[1912.03053](#)].
- [25] N. Hüsken, R.E. Mitchell and E.S. Swanson, *K-matrix analysis of e^+e^- annihilation in the bottomonium region*, *Phys. Rev. D* **106** (2022) 094013 [[2204.11915](#)].
- [26] E. van Beveren and G. Rupp, *Modern meson spectroscopy: the fundamental role of unitarity*, *Prog. Part. Nucl. Phys.* **117** (2021) 103845 [[2012.03693](#)].
- [27] J. Tarrús Castellà and E. Passemar, *Exotic to standard bottomonium transitions*, *Phys. Rev. D* **104** (2021) 034019 [[2104.03975](#)].
- [28] N. Brambilla, S. Eidelman, C. Hanhart, A. Nefediev, C.P. Shen, C.E. Thomas et al., *The XYZ states: experimental and theoretical status and perspectives*, *Phys. Rept.* **873** (2020) 1 [[1907.07583](#)].
- [29] A. Ali, L. Maiani, A.Y. Parkhomenko and W. Wang, *Interpretation of $\Upsilon_b(10753)$ as a tetraquark and its production mechanism*, *Phys. Lett. B* **802** (2020) 135217 [[1910.07671](#)].
- [30] P. Bicudo, N. Cardoso, L. Mueller and M. Wagner, *Computation of the quarkonium and meson-meson composition of the $\Upsilon(nS)$ states and of the new $\Upsilon(10753)$ Belle resonance from lattice QCD static potentials*, *Phys. Rev. D* **103** (2021) 074507 [[2008.05605](#)].
- [31] P. Bicudo, N. Cardoso, L. Mueller and M. Wagner, *Study of $I = 0$ bottomonium bound states and resonances in $S, P, D,$ and F waves with lattice QCD static-static-light-light potentials*, *Phys. Rev. D* **107** (2023) 094515 [[2205.11475](#)].

- [32] Z.G. Wang, *Vector hidden-bottom tetraquark candidate: $\Upsilon(10750)$* , *Chin. Phys. C* **43** (2019) 123102 [[1905.06610](#)].
- [33] K. Akai, K. Furukawa and H. Koiso, *SuperKEKB collider*, *Nucl. Instrum. Meth.* **A907** (2018) 188 [[1809.01958](#)].
- [34] BELLE II collaboration, *Belle II technical design report*, [1011.0352](#).
- [35] BELLE II SVD collaboration, *The design, construction, operation and performance of the Belle II silicon vertex detector*, *JINST* **17** (2022) P11042 [[2201.09824](#)].
- [36] BELLE II TRACKING GROUP collaboration, *Track finding at Belle II*, *Comput. Phys. Commun.* **259** (2021) 107610 [[2003.12466](#)].
- [37] D. Kotchetkov et al., *Front-end electronic readout system for the Belle II imaging Time-Of-Propagation detector*, *Nucl. Instrum. Meth. A* **941** (2019) 162342 [[1804.10782](#)].
- [38] BELLE II FRAMEWORK SOFTWARE GROUP collaboration, *The Belle II Core Software*, *Comput. Softw. Big Sci.* **3** (2019) 1 [[1809.04299](#)].
- [39] BELLE II collaboration, “Belle II Analysis Software Framework (basf2).” <https://doi.org/10.5281/zenodo.5574115>.
- [40] S. Agostinelli et al., *GEANT4 - A Simulation Toolkit*, *Nucl. Instrum. Meth. A* **506** (2003) 250.
- [41] D.J. Lange, *The EvtGen particle decay simulation package*, *Nucl. Instrum. Meth.* **A462** (2001) 152.
- [42] G. Rodrigo, H. Czyz, J.H. Kuhn and M. Szopa, *Radiative return at NLO and the measurement of the hadronic cross-section in electron positron annihilation*, *Eur. Phys. J. C* **24** (2002) 71 [[hep-ph/0112184](#)].
- [43] E. Barberio, B. van Eijk and Z. Was, *PHOTOS: A Universal Monte Carlo for QED radiative corrections in decays*, *Comput. Phys. Commun.* **66** (1991) 115.
- [44] G. Balossini, C.M. Carloni Calame, G. Montagna, O. Nicrosini and F. Piccinini, *Matching perturbative and parton shower corrections to Bhabha process at flavour factories*, *Nucl. Phys. B* **758** (2006) 227 [[hep-ph/0607181](#)].
- [45] G. Balossini, C. Bignamini, C.M.C. Calame, G. Montagna, O. Nicrosini and F. Piccinini, *Photon pair production at flavour factories with per mille accuracy*, *Phys. Lett. B* **663** (2008) 209 [[0801.3360](#)].
- [46] G. Rodrigo, H. Czyz, J.H. Kuhn and M. Szopa, *Radiative return at NLO and the measurement of the hadronic cross-section in electron positron annihilation*, *Eur. Phys. J. C* **24** (2002) 71 [[hep-ph/0112184](#)].
- [47] F.A. Berends, P.H. Daverveldt and R. Kleiss, *Complete Lowest Order Calculations for Four Lepton Final States in electron-Positron Collisions*, *Nucl. Phys. B* **253** (1985) 441.
- [48] F.A. Berends, P.H. Daverveldt and R. Kleiss, *Monte Carlo Simulation of Two Photon Processes. 2. Complete Lowest Order Calculations for Four Lepton Production Processes in electron Positron Collisions*, *Comput. Phys. Commun.* **40** (1986) 285.
- [49] Y. Iwasaki, B. Cheon, E. Won, X. Gao, L. Macchiarulo, K. Nishimura et al., *Level 1 trigger system for the Belle II experiment*, *IEEE Trans. Nucl. Sci.* **58** (2011) 1807.
- [50] BELLE II collaboration, “OrcaKinFit: Kinematic fitting library for basf2.” <https://github.com/tferber/OrcaKinFit>, 2024.

- [51] BELLE II collaboration, *Observation of $e^+e^- \rightarrow \eta\Upsilon(2S)$ and search for $e^+e^- \rightarrow \eta\Upsilon(1S), \gamma X_b$ at \sqrt{s} near 10.75 GeV*, [2509.01917](#).
- [52] BELLE collaboration, *Observation of anomalous $\Upsilon(1S)\pi^+\pi^-$ and $\Upsilon(2S)\pi^+\pi^-$ production near the $\Upsilon(5S)$ resonance*, *Phys. Rev. Lett.* **100** (2008) 112001 [[0710.2577](#)].
- [53] W. Sun, T. Liu, M. Jing, L. Wang, B. Zhong and W. Song, *An iterative weighting method to apply ISR correction to e^+e^- hadronic cross-section measurements*, *Front. Phys. (Beijing)* **16** (2021) 64501 [[2011.07889](#)].
- [54] M. Benayoun, S.I. Eidelman, V.N. Ivanchenko and Z.K. Silagadze, *Spectroscopy at B factories using hard photon emission*, *Mod. Phys. Lett. A* **14** (1999) 2605 [[hep-ph/9910523](#)].
- [55] BELLE II collaboration, *Measurement of the integrated luminosity of data samples collected during 2019-2022 by the Belle II experiment*, *Chin. Phys. C* **49** (2025) 013001 [[2407.00965](#)].
- [56] M.J. Oreglia, *A Study of the Reactions $\psi' \rightarrow \gamma\gamma\psi$* , Ph.D. thesis, Stanford University, Dec, 1980.
- [57] J. Segovia, P.G. Ortega, D.R. Entem and F. Fernández, *Bottomonium spectrum revisited*, *Phys. Rev. D* **93** (2016) 074027 [[1601.05093](#)].
- [58] J.-Z. Wang, Z.-F. Sun, X. Liu and T. Matsuki, *Higher bottomonium zoo*, *Eur. Phys. J. C* **78** (2018) 915 [[1802.04938](#)].
- [59] S. Godfrey and K. Moats, *Bottomonium Mesons and Strategies for their Observation*, *Phys. Rev. D* **92** (2015) 054034 [[1507.00024](#)].